Dynamics on Individual Reaction Sites in Steady-State Carbon Monoxide Oxidation on Stepped Platinum(113)

Gengyu Cao, Md. Golam Moula, Yuichi Ohno, and Tatsuo Matsushima*

Catalysis Research Center, Hokkaido University, Sapporo 060-0811, Japan

Received: November 17, 1998; In Final Form: February 15, 1999

The reaction kinetics and dynamics of carbon monoxide oxidation on a stepped Pt(113) = (s)2(111) × (001) surface were studied by angle-resolved kinetic and velocity measurements at the steady state. CO_2 desorption sharply collimated nearly along either the (111) site normal or the (001) site normal. Only two reaction sites, the (111) and (001) sites, were operative. The translational energy of CO_2 was characteristic of each site throughout a site switching. At surface temperatures above 520 K in the active region, where the reaction was first order in CO, the preference of the (111) site was suppressed with increasing CO pressure. Below 520 K, on the other hand, site switching slowly took place under limited conditions, in which both sites considerably contributed to the reaction and a meta-stable adsorbed phase seemed to be formed. The preference for the (111) site over the (001) site was caused by the former's higher reactivity of oxygen.

I. Introduction

A surface reaction consists of several elementary processes, which are often sensitive to surface structures. To understand the whole reaction scenario, it is of critical importance to study the kinetics and dynamics of each process on individual reaction sites in addition to their cooperative behavior. The spatial and velocity distributions of desorbing products provide the dynamics of key processes involved in the product formation event as well as structural information of reaction sites. These work well even when the overall reaction rate is controlled by reactant adsorption and then the interaction between adsorbates is obscured in kinetic studies at the steady state.[1] The observation of site-switching will yield an insight into the relation of the rate-determining step to the site preference. This kind of observation is now possible in steady-state CO oxidation on a stepped Pt(113) surface because two kinds of reaction sites are operative and the product desorption can be separately examined on each site.[2,3] This paper proposes a model in which two different reaction sites cooperatively work to receive reactants and site preference sharply changes under the conditions close to the switching point of the rate-determining step.

In CO oxidation on noble metals at the steady state, oxygen and CO molecules first adsorb as O(a) and CO(a), and then the reaction subsequently proceeds via a Langmuir−Hinshelwood mechanism, i.e., $CO(a) + O(a) \rightarrow CO_2(g)$.[4] The product CO_2 carries a high energy in translational and internal modes.[5−8] The reaction site for CO_2 formation can be identified by the spatial and velocity distributions of the desorbing product because of its highly repulsive desorption.[1,9] Some research has already been published on the dynamics on individual sites by using AR-TDS (angle-resolved thermal desorption spectroscopy) combined with the TOF (time-of-flight) technique.[10−14] In such TDS work, however, the coverage of CO(a) and O(a) decreases with increasing surface temperature, as these are removed as CO_2. It is difficult to study either the coverage effect at fixed temperatures, or the temperature effect at fixed coverages. Furthermore, the reactant adsorption process is always omitted. Under steady-state conditions, on the other hand, the reaction dynamics will be examined at fixed temperatures and constant surface coverages.[3]

A critical CO pressure, where the rate-determining step switches from the CO adsorption to oxygen dissociative adsorption, is commonly observed in steady-state CO oxidation on platinum metals.[15−18] Below the critical pressure, the surface is fairly covered by oxygen (O(a)). CO(a) becomes predominant above the critical pressure, and oxygen adatoms decrease to negligible amounts, i.e., from O(a) > CO(a) to O(a) ≪ CO(a) with increasing CO pressure. This change is caused by the above switching of the rate-determining step under the condition that the process of $CO(a) + O(a) \rightarrow CO_2(g)$ occurs much faster than the adsorption of either CO or oxygen.[15,18] Nevertheless, adsorbed CO has a chance to interact with oxygen on each site, since the surface residence time of CO until the removal as CO_2 is approximately a few hundred microseconds, much longer than the residence time on each adsorption site.[19−21] Thus, the former region of O(a) > CO(a) provides a stage suitable for the examination of site preference, one in which oxygen is more reactive toward CO when different kinds of oxygen are on the surface. A site-switching analysis will provide transfer phenomena of surface reactants in the course of catalyzed reactions.

AR-TDS has been applied to both site identification and switching in the CO oxidation on stepped surfaces, Pt(112), (113), (335), and (557).[2,11−14,22−25] The resultant CO_2 spatial distribution shows that the product is desorbed from narrow terraces or steps. On Pt(113), CO_2 is predominantly formed on the (111) site at high CO(a) coverage, while at high O(a) coverage, the contribution from the (001) site is enhanced and the site preference is reversed. The site preference at low temperatures is not merely controlled by the reactivity of oxygen because of the limited surface mobility of CO.[2]

Two kinds of oxygen adsorption sites, suitable for CO oxidation, were proposed on Pt(113) in AR-TDS work,[2,22] i.e., the 3-fold hollow sites on (111) facets and the 4-fold hollow sites on (001) steps. The former declines 29.5°, whereas the latter inclines 25.2° in the opposite direction. A top view and a

* Corresponding author. Fax: +81-11-706-3695.

10.1021/jp984438l CCC: $18.00
Published on Web 04/02/1999

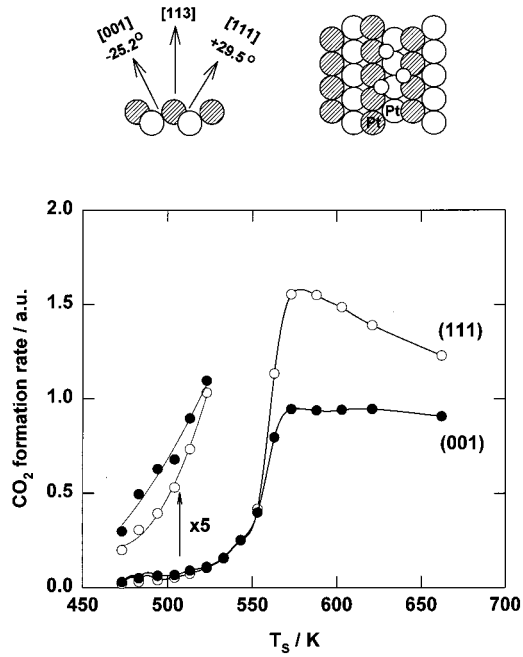

Figure 1. Variation of the steady-state CO_2 signal at both $\theta = +22°$ for the (111) site and $\theta = -20°$ for the (001) site with surface temperatures at fixed $P_{O_2} = 3 \times 10^{-5}$ Torr and $P_{CO} = 1.5 \times 10^{-5}$ Torr. Both top and side views of Pt(113) are shown in the upper panel. The small circles indicate oxygen adsorption sites.

side view of the surface are schematically shown in the upper panel in Figure 1. The CO_2 formation on each reaction site can be studied in angle-resolved measurements.

II. Experimental Section

The apparatus has been described in detail elsewhere.[26] It consists of three chambers, which are evacuated by individual pumping systems. The reaction chamber has RV-LEED (reverse-view low-energy electron diffraction) and XPS (X-ray photoelectron spectroscopy) optics, a QMS (quadrupole mass spectrometer), an Ar^+ gun, a sample manipulator, and a gas handling system. The chopper chamber has a 1.5 mm × 6 mm rectangular slit toward the reaction chamber as well as a time-correlation random chopper system with slots of equal width (1 mm × 6 mm) distributed in a pseudorandom sequence (with a double sequence of 255 elements each).[27] The analyzer chamber is equipped with a QMS operating in a pulse-counting mode. A 50 mm long drift tube with an inner diameter of 4 mm is inserted between the chopper chamber and the analyzer.[28] The distance between the sample and the ionizer of the QMS is 400 mm, and the distance from the chopper blade to the ionizer is 377 mm. The aperture diameter of the ionizer is only 6 mm. These make the acceptance angle of 1.0°. A time resolution of 20 μs is obtained in velocity measurements with the chopper rotating speed of 98.032 Hz.[27]

A Pt(113) single crystal of 10 mm diameter and 1 mm thickness (supplied by MaTeck, Germany) was mounted on top of the manipulator. The surface was cleaned by the standard routine.[2] At this stage, the LEED image showed a (1 × 1) pattern. The partial pressures of CO (P_{CO}) and O_2 (P_{O_2}) were kept constant by dosing gases continuously through leak valves. The crystal was rotated to change the desorption angle (θ, polar angle) in a plane perpendicular to the step edge. The desorption angle was defined positive, as it was upward for the (001) steps (step-up), and negative in the downward direction (step-down).

III. Results

A. Temperature Dependence. The steady-state CO_2 formation rate was monitored in angle-resolved form by the QMS in the analyzer chamber as well as in angle-integrated form by the other QMS in the reaction chamber. The rate in the former was observed as the difference between the CO_2 signal at the desired surface temperature and that when the crystal was moved away from the line of sight position. The total CO_2 signal in the latter case was measured as the difference in the angle-integrated signal between the desired surface temperature and room temperature. The resultant kinetics in angle-resolved form depended on the desorption angle and was characterized by angle-dependent reaction orders. Since the product desorption collimated either along $\theta = -20°$ or $\theta = +22°$, as shown in section C, the formation rate was mostly measured at these angles except for angle-dependence work.

Typical surface temperature (T_s) dependence of the CO_2 formation rate in the above two directions is shown in Figure 1, where P_{CO} was kept at 1.5×10^{-5} Torr and P_{O_2} at 3.0×10^{-5} Torr. The rate was negligible below $T_s = 400$ K. It slowly increased below 550 K and rapidly above 550 K to a maximum with increasing T_s before decreasing at higher values. At low temperatures (<530 K), the CO_2 desorption rate in the $-20°$ direction, indicated by (001), was higher than that at $\theta = +22°$, shown by (111). Above this temperature, the latter overcame the former. The maximum position shifted to high T_s values with increasing total pressure as long as P_{CO} was close to P_{O_2}.

B. CO Pressure Effect. P_{CO} dependence was characterized by sharp kinetic transitions at a critical P_{CO} value. Above the value, the reaction was retarded by CO, showing negative orders. The region with P_{CO} lower than the critical value is named the "active region", and that with P_{CO} higher than the critical value is called the "inhibited region." The reaction rate observed in angle-integrated form was insensitive to T_s in the active region, whereas it was sensitive in the inhibited region. In the former, the reaction was first order in CO. On the other hand, in the latter, CO retarded the reaction more strongly at lower temperatures. The critical CO pressure shifted to lower values with decreasing T_s. These are consistent with the literature.[15−18]

In angle-resolved measurements, significant differences were found in P_{CO} dependence between $\theta = -20°$ and $+22°$. The results at various T_s values are shown in Figure 2. The reaction order with respect to CO (the slope of the lines in the figure) was far from unity and shifted toward unity with decreasing T_s from smaller values at $\theta = +22°$ and from higher values at $\theta = -20°$. At $T_s > 520$ K in the active region, the reaction order at $-20°$ was higher than unity, whereas the value at $+22°$ was less than unity. At $T_s < 520$ K, the reaction order difference became smaller, and the two lines were almost parallel. Above 530 K, the CO_2 formation observed at $+22°$ was overwhelmed by that at $-20°$ fairly below the critical CO pressure. Nevertheless, the kinetics at both angles showed common critical CO pressures. It should also be noticed that the CO_2 signal at $+22°$ showed a limited value between the crossing point and the critical P_{CO} value.

At $T_s = 500$ K or below, we observed a "hysteresis"; i.e., once inhibited, the reaction was still maintained even if P_{CO} was decreased to a value corresponding to the active region, as shown in the bottom panel of the figure.

C. Angular Distribution. The angular distribution was measured in a plane perpendicular to the step edge and not parallel to it. This is because, in the latter case, CO_2 desorption peaked simply along the bulk surface normal.[2,22] The distributions in the former azimuth were fairly different in the two

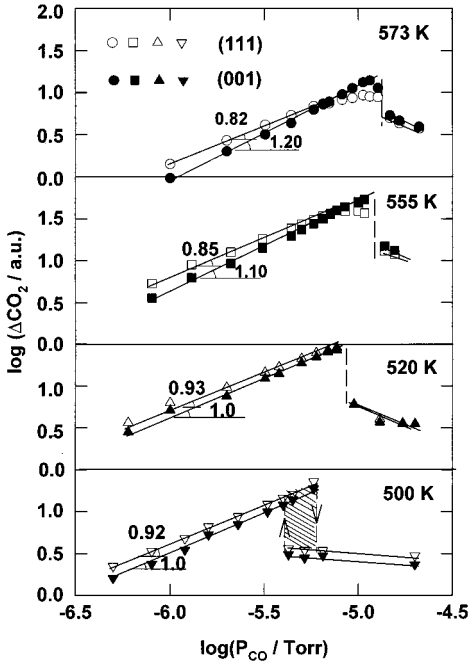

Figure 2. P_{CO} dependence of the steady-state CO_2 signal observed at both $\theta = +22°$ for the (111) site and $\theta = -20°$ for the (001) site at various surface temperatures. P_{O_2} was fixed at 3×10^{-5} Torr. The dashed lines show kinetic transitions. The inserted figures indicate the reaction order with respect to CO.

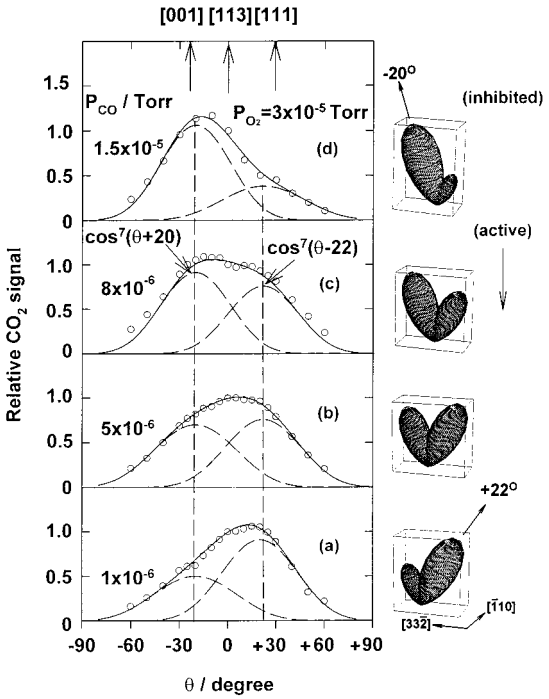

Figure 3. Angular distributions of desorbing CO_2 in a plane perpendicular to the step edge at different P_{CO} values and at $P_{O_2} = 3 \times 10^{-5}$ Torr and $T_s = 555$ K. The right column shows a three-dimensional polar coordinate representation of the distributions.

regions. Typical angular distributions are shown in Figure 3. The distribution shape changed with increasing P_{CO}. The desorption collimated sharply around $\theta = +22°$ in the active region far below the critical CO pressure and showed a small shoulder around $-20°$ (Figure 3a). The former component was relatively suppressed at higher CO pressures, where the latter was rapidly enhanced (Figure 3b,c). In the inhibited region

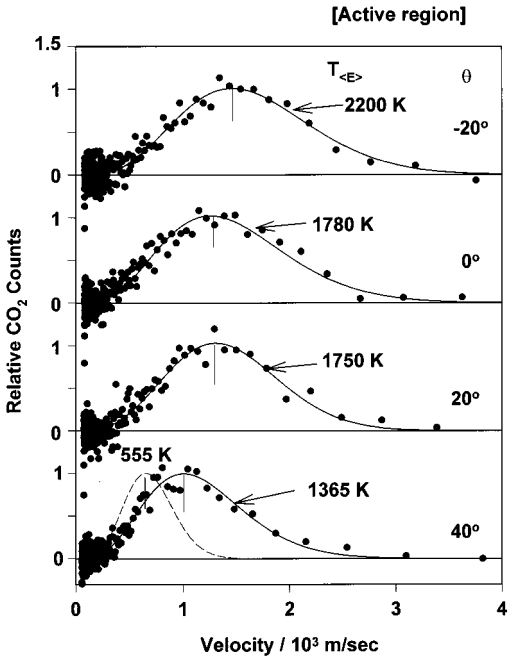

Figure 4. Velocity distributions of CO_2 at different desorption angles in the active region of $P_{O_2} = 3 \times 10^{-5}$ Torr, $P_{CO} = 6 \times 10^{-6}$ Torr, and $T_s = 555$ K. The solid curves are modified Maxwellian distributions obtained by curve fitting. The broken curve indicates a Maxwell distribution at the surface temperature. The vertical bars show the maximum flux positions.

(Figure 3d), CO_2 desorption collimated mostly at around $-20°$ although the former component was still significant.

The distribution curves were deconvoluted into two simple power functions of cosine of the desorption angle. The distribution was well approximated by a linear combination of $\cos^7(\theta + 20)$ and $\cos^7(\theta - 22)$ components, as shown by the broken curves. The resultant distributions of each component were broader than those in TDS work probably because of elevated surface temperatures.[2] Their sum was drawn by the solid curves. The collimation angle was estimated to be $-20 \pm 2°$ and $+22 \pm 2°$. The former value slightly shifted from the (001) step normal of $-25.2°$ and the latter from the (111) terrace normal of $+29.5°$. The former was assigned to the reaction on the (001) site and the latter to that on the (111) site, respectively. The linear plot used in this figure hardly provides the real image of the spatial distribution because the signal at high angles is artificially enhanced and both components are overlapped. For an easy view, the spatial distributions of each desorption component are displayed in three-dimensional polar coordinates in the right column of Figure 3. In this drawing, a symmetric distribution is assumed around the collimation axis, and the distribution in the [110] direction is referred to the results in TDS work.[2] A clear preference change can be seen in the enhanced component along the [001] direction with increasing P_{CO} below the critical value.

D. Kinetic Energy. Both (111) and (001) sites produced CO_2 with characteristic translational energies, although the value also depended on the CO pressure, the surface temperature, and the desorption angle as well. Typical velocity distributions of CO_2 at various desorption angles are shown in Figure 4, where P_{CO} was fixed at 6×10^{-6} Torr and P_{O_2} was 3×10^{-5} Torr, i.e., in the active region. The distributions largely shifted from a Maxwellian form expected at the surface temperature of 555 K (the broken line). The translational temperature defined as $T_{\langle E \rangle} = \langle E \rangle / 2k$ was derived from curve fitting to a modified Maxwellian form. $\langle E \rangle$ is the mean translational energy, and k, the

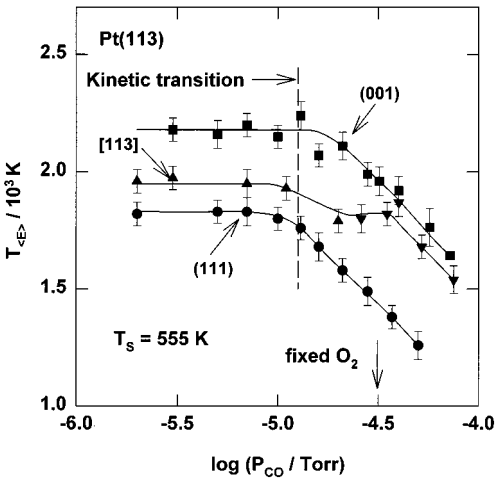

Figure 5. P_{CO} dependence of the translational energy of CO_2 at $P_{O_2} = 3 \times 10^{-5}$ Torr. (111) and (001) indicate the value for CO_2 desorbed at $\theta = +22°$ and $\theta = -20°$, respectively. The value for the normal desorption is shown by [113].

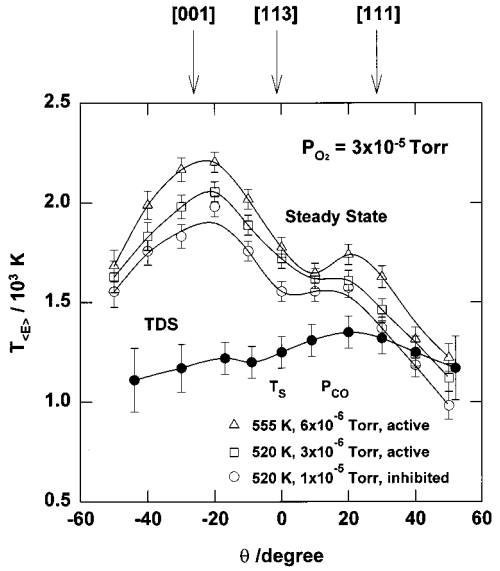

Figure 6. Angle dependence of the translational energy of CO_2 in both the active (□, △) and inhibited (○) regions. The closed circles indicate the energy determined in TDS work at $T_s = 300$ K.[13]

Boltzmannn constant. The modified Maxwellian distribution[10,29] is written as

$$f(v) = v^3[-(v - v_o)^2/\alpha^2] \quad (1)$$

where v is the velocity of the molecule, v_o is the stream velocity, and α is a width parameter. The distribution shape was very close to the Maxwellian form because the normalized speed ratio S was close to unity. This quantity is defined as[29]

$$S = (\langle v^2\rangle/\langle v\rangle^2 - 1)^{1/2}/(32/9\pi - 1)^{1/2} \quad (2)$$

where $\langle v\rangle$ is the mean velocity and $\langle v^2\rangle$ is the mean square velocity.

The resultant $T_{\langle E\rangle}$ value is shown as a function of P_{CO} in Figure 5 and of the desorption angle in Figure 6. At low CO pressures, the value was 2200 ± 50 K for CO_2 observed at $\theta = -25°$ indicated by (001) and remained fairly constant with P_{CO}, beginning to decrease just above the critical CO pressure. On the other hand, the translational temperature at $\theta = +20°$, as shown by (111), was 1700 ± 50 K and decreased rapidly above the critical CO. The value for CO_2 in the normal direction was around 1900 K and shifted closely to the value at $\theta = -25°$ above the critical P_{CO}.

The $T_{\langle E\rangle}$ value decreased quickly upon an increase in the shift from the collimation angle in both reaction regions, as shown in Figure 6. The reaction was in the active region at $P_{CO} = 3 \times 10^{-6}$ Torr and $P_{O_2} = 3 \times 10^{-5}$ Torr at $T_s = 520$ K and in the inhibited region with $P_{CO} = 1 \times 10^{-5}$ Torr. The $T_{\langle E\rangle}$ value was commonly maximized both at around $\theta = -25°$ and $+20°$, although the angular distributions were quite different (see Figure 3). These values increased slightly with increasing surface temperature (Figure 6).

IV. Discussion

A. Reaction Site. CO_2 formation takes place on both (111) terrace sites and (001) step sites because the angular distribution consists of only two desorption components collimated closely to the (111) site normal and the (001) site normal. Furthermore, the translational energy is maximized at these angles. The repulsive force exerted from the site toward CO_2 is directed in these directions.

The CO oxidation process on platinum metals is likely to take place on oxygen adsorption sites since the mobility of CO is much higher than that of oxygen adatoms.[21] The reactant oxygen adatom does not seem to move significantly from the adsorption site during the reaction event. Recent theoretical work by Alavi et al. shows that oxygen moves from the 3-fold hollow site toward the nearest bridged site and returns to the original site during the reaction event on Pt(111).[30] The reaction may not take place at the center of the oxygen adsorption site but rather around it. However, CO_2 desorption is still expected to collimate along the normal of the site plane. On the present surface, one kind of 4-fold hollow sites is found on (001) facets, and two kinds of 3-fold hollow sites (fcc and hcp sites) are found on (111) facets (Figure 1). These hollow sites are suitable for oxygen adsorption and can act as reaction sites for CO_2 formation.

In the above site assignment, the collimation angles are still shifted about 5° and 7° from the [001] and [111] directions toward the bulk surface normal, respectively. The extent is about 25% of the declining angle of the site plane from the bulk surface plane, which is reasonably compared with those on other stepped surfaces.[1,9] Several factors were considered as contributing to this shift. The first is *surface distortions*, where surface top atoms are moved toward the bulk crystal from the position expected in the bulk. For example, from LEED I/V analysis, the (111) terrace was concluded to decline about ±30° on Pt(110)(1 × 2) although it would decline ±35.2° without distortions.[31] The second is the "*smoothing effect*" induced by conduction electrons.[32] The electronic surface exerting a repulsive force will be less corrugated by localization of electrons around positively charged steps. The repulsive force toward CO_2 may not be exactly along the reaction site normal. Moreover, the momentum transfer from the rotational motion into the translational modes may change the desorption trajectory. It is difficult to evaluate each factor separately. However, the shift from the site normal was mostly suppressed for CO_2 with a high velocity in photolytic CO oxidation.[33] This suggests a significant contribution from the smoothing effect.

The surface structure was not analyzed in the course of the catalyzed reaction. The surface might be reconstructed into a missing-row structure, as proposed on Pd(113), i.e., into a (s)3-(111) × 3(001) form.[34] The above site assignment, however, is still valid even when the surface is reconstructed in this way because no change is expected in the orientation of both facets.

B. Reaction Kinetics. The reaction site preference changed sharply with increasing surface temperature, as shown in Figure 1. The contribution from the (001) site was more than that from the (111) site below $T_s = 540$ K, where the total CO_2 formation was considerably suppressed. The reaction rate was controlled by oxygen dissociation, which is retarded by CO. Above this temperature, the CO_2 formation steeply increased because the CO(a) removal was enhanced through increased CO_2 formation and thermal desorption. The reaction on the (111) site was enhanced sharply, more than on the other site, and then the site preference was eventually reversed. The reaction rate was determined by CO adsorption, and the surface was mostly covered by oxygen. The preference of the (111) site indicates a higher reactivity of oxygen on this site. The rate rapidly decreased on the (111) site with increasing T_s after the maximum position, although it remained invariant on the (001) site. This suggests a transfer of oxygen from the (001) site to the (111) site under the condition that oxygen be rapidly removed on the latter. Wang et al. found that above 400 K, an exchange of oxygen was equilibrated between (001) steps and (111) terraces on Pt(533) = (s)4(111) × (001).[35]

The site switching becomes clearer in P_{CO} dependence because surface species change sharply toward the critical CO pressure. The kinetics of the rate *in angle-integrated form* changed sharply from nearly first order to negative orders at the critical pressure. This change has been explained by a switching of the rate-limiting step from the CO adsorption to oxygen dissociation.[15−18] It is well-known that in the active region, O(a) is much more than CO(a). Most of the incident CO is converted into CO_2. At a critical P_{CO} value, CO(a) quickly increases to the level equilibrium with the gas phase, and above the P_{CO} value, it retards oxygen adsorption, yielding negative orders. In the resultant inhibited region, O(a) is much less than CO(a). In this phenomenological description, the surface as well as adsorbed species are considered to be uniform, and no information on the reaction sites can be obtained.

In angle-resolved desorption measurements, the reaction order can be separately examined on each reaction site, and then the cooperative relation of different reaction sites can be studied. The collision number of CO or O_2 may be approximately equal on both sites, since the area of (111) and (001) facets is close. Incident CO adsorbs with a sticking probability close to unity and is distributed on both sites.[36,37] No significant difference is expected in the kinetic behavior of adsorbed CO on both sites at high temperatures, because the residence time on each site is very short due to the extremely high surface mobility.[21,38] On the other hand, oxygen adatoms may be populated in a different way. Oxygen atoms first cover the (001) site. This is because the intermediate O_2(a) is highly mobile (the binding energy being less than 10 kcal/mol[39,40]) and its dissociation mostly proceeds on this site.[35,41] In addition, it is the results of the binding energy on the 4-fold hollow sites being higher than that on the 3-fold hollow sites on the (111) terrace.

C. Site Switching. In the active region with $P_{O_2} \gg P_{CO}$, both sites are highly covered by O(a).[16,17] The CO_2 formation rate on the (111) site was faster than that on the (001) site. This confirms a higher reactivity of oxygen on this site, consistent with a smaller binding energy. The limiting ratio of the amount of CO_2 formed on the (111) to that on the (001) was estimated to be about 3 by extrapolating the value determined from the angular distribution to $P_{CO} = 0$. This may be the reactivity difference of oxygen between the two sites, since the oxygen density is similar. With increasing incident CO in the active region, more oxygen was removed as CO_2 from the (111) site than the (001) site. The population of oxygen should decrease on the (111) site more rapidly than on the other. This became clear when P_{CO} was close to the kinetic transition value where O(a) rapidly decreased. The CO_2 formation on the (111) site cannot linearly increase with increasing P_{CO} because of the rapid decrease of oxygen. This yields the reaction order with respect to CO less than unity. The remaining CO(a) on the (111) site must diffuse to the (001) site and be removed as CO_2. Eventually, the reaction order on the (001) site increased more than unity.

This cooperative function by both sites affects the site preference and causes common critical CO pressures. At high temperatures, a large difference in the reaction order to CO is expected between the two sites. This is because oxygen diffusion is fast and site cooperation is effective. Furthermore, the total amount of oxygen is decreased, and the oxygen population is subsequently shifted more to the (001) site with a higher binding energy. With decreasing T_s, the difference in the reaction order is attenuated because the total oxygen coverage must increase to keep the removal rate of CO constant, irrespective of a decrease of the rate constant for the CO_2 formation. In fact, the activation energy of this process is approximately 25 kcal/mol.[20] Eventually, oxygen is highly populated on both sites in the active region. Thus, no site switching takes place.

In the inhibited region, where CO prevents oxygen from adsorbing and retards the reaction, the overall reaction rate is controlled by the dissociative adsorption of O_2. O(a) is removed as CO_2 immediately after formation and maintained at a much lower level than CO(a). Hence, CO_2 formation takes place mostly on the (001) site. In fact, the ratio of the amount of CO_2 formed on the (111) to that on the (001) was estimated to be about 0.1. However, this site switching becomes unclear at low temperatures, where CO and oxygen form separate domains. The local coverage of each reactant cannot be controlled by the average value over the whole surface. At lower temperatures, the kinetics showed a hysteresis reminiscent of chemical oscillation.[42] At high CO and oxygen pressure suitable to surface phase transition, oscillation takes place near the kinetic transition.[43] CO and oxygen are likely to form separate domains. Both oxygen and CO mobilities must decrease, and the above cooperative mechanism becomes less effective.

Nevertheless, the critical pressure was always observed at common P_{CO} values on both sites. This suggests that CO and oxygen are quickly supplied from the (111) site or the (001) to the other, leading both sites into the inhibited region whenever either site is deficient in oxygen adatoms. Hence, site switching is sensitive to the difference in coverage, surface mobility, and the reactivity of oxygen between the two sites as well. On the other hand, the switching in the rate-determining step is controlled by the difference of the reactant supply onto the whole surface.

D. Velocity and Site. The desorption angle dependence of the translational energy shows which direction the repulsive force is exerted from the working site. The energy peaked at $\theta = -20$ to $-25°$ and $\theta = +20$ to $+30°$ irrespective of the reaction region. The two reaction sites yielded a product with highly different translational energies, 2200 K (∼9 kcal/mol) and 1700 K (∼7 kcal/mol). This difference was kept invariant with increasing CO pressure, although the energy itself decreased above the critical P_{CO} value (Figure 5). Each reaction site characterizes the translational energy. With decreasing P_{CO}, the energy was constant below the critical value, where the oxygen coverage changed rapidly, indicating that the energy does not depend on the oxygen density. On the other hand, the

energy decreased quickly with increasing P_{CO} in the inhibited region, indicating that the CO(a) density affects the translational energy. The energy of CO_2 observed in the bulk surface normal was constant below the critical CO pressure. Above the value, it shifted toward the energy for CO_2 from the (001). The CO_2 in the normal direction involved both the components from the (111) and (001) sites, and their contribution varied with CO pressure. It mostly contained the product from the (001) in the inhibited region.

Furthermore, the translational energy at the steady state was in high contrast to that in TDS work.[13,14] The closed circles in Figure 6 show the $T_{\langle E \rangle}$ value in TDS procedures around 300 K. The value was slightly less around $-20°$ than that at $+20°$. Thus, a large difference of about 1000 K ($\sim$4 kcal/mol) was found on the (001) site, and a lower difference of 200−400 K was noticed on the (111) site. The latter value can be fully explained by the surface temperature effect because of an about 250 K difference in the surface temperature between the two experiments.[26] On the other hand, the former difference is too large to be explained by the temperature effect alone.

Additionally, the collimation angle of the CO_2 desorption showed also a significant difference, i.e., $\theta = -20°$ at the steady state and $\theta = -17$ to $-15°$ in TDS. This suggests the modification of the (001) site under the steady-state conditions. In fact, TDS work combined with isotope tracers by Akiyama et al. showed that the (001) site was easily modified by subsurface oxygen and that the oxygen reactivity was not completely lost on the resultant modified sites.[44] These researchers also showed that oxygen on the modified site had a lower binding energy. Under the steady-state conditions in oxygen atmosphere at high temperatures, this subsurface oxygen may be formed. Similar modifications were directly observed by PEEM on a Pt(110) surface.[45,46]

The activated state for CO_2 formation may be raised on the modified site and yield the product with a higher energy. Two models may be considered for CO_2 velocity enhancement, i.e., changes in the energy partition itself or in the repulsive force exerted from the site. The potential energy of the activated state of CO_2 formation has been estimated to be about 30 kcal/mol on Pt(111) above the vacuum level.[20] This energy is partitioned into the translational and internal modes of CO_2 as well as into surface modes. The energy disposal may change on modified sites because surface lattices are distorted or relaxed during reaction events. The insertion of oxygen beneath the surface may reduce the energy transfer to the crystal lattice. The potential energy of the activated state itself may increase with decreasing distance from the surface plane because the force between nascent CO_2 and the surface is due to the Pauli repulsion.[1,9]

Translational energy decreased quickly with increasing CO pressure above the critical CO value. This decrease has already been reported on Pt(557) and Pt(133).[26,47] There must be a mechanism in which energy transfer is efficient when the surface is covered by a significant amount of CO. The collision between CO_2 and CO might yield a more efficient energy flow than that between CO_2 and Pt because of a smaller difference in the mass mismatch.

Translational energy is only a part of the total energy released when CO_2 is formed as described above. The translational energy measured in this study is 7−9 kcal/mol, only about one-fourth of the total energy. Kunimori and co-workers found that internal energy ranged 5−8 kcal/mol on Pd(111), Pd(110), Pt(111), Pt(110)(1 × 2), and Pd(335), depending on the surface material, structure, and temperature.[48−53] The total energy, which is carried out by CO_2, is predicted to increase with increasing temperature if the value measured at high reactant pressures and high surface temperatures can be compared with the present results. This increase is still possible because the energy partitioned into the CO_2 molecule is about 50% of the total energy and, furthermore, because the energy transferred into the surface may be reduced at high temperatures, as predicted from smaller accommodation coefficients at elevated temperatures.[54] However, the energy partitioned into the surface modes is not certain yet.[55]

V. Summary

Angle-resolved kinetic and velocity measurements of desorbing product CO_2 were performed in steady-state CO oxidation on a stepped Pt(113) = (s)2(111) × (001) surface. The results are summarized as follows.

1. The CO_2 desorption sharply collimates along either the (111) site normal or the (001) site normal. Both the (111) and (001) sites are operative for CO_2 formation.

2. The translational energy of CO_2 peaks at these collimation angles and confirms the site assignment.

3. At surface temperatures above 520 K in the active region, the preference of the (111) site is suppressed with increasing CO pressure. This preference over the (001) site is caused by a higher reactivity of oxygen on the former than on the latter.

4. Below 520 K, site switching takes place slowly under limited conditions, where both sites contribute considerably to the reaction and a meta-stable adsorbed phase appears to be formed.

5. The translational energy is characteristic of each site throughout the site switching.

Acknowledgment. The authors thank Ms. Atsuko Hiratsuka for her drawings in 3-dimensional polar coordinates. Md. Golam Moula is indebted to the Ministry of Education, Science, Sports, and Culture of Japan for a scholarship for 1998−1999. This work was partly supported by a COE special equipment program in 1996 of the above Ministry and also a Grant-in-Aid (No. 06403012) for General Scientific Research from the said Ministry.

Appendix

In angle-resolved desorption measurements, the signal observed with a mass spectrometer is not simply related to the total flux of product molecules from each site, even if the signal is corrected from the density into the flux unit by considering the velocity. This is because the relation between the observed signal and the total flux depends on the desorption angle and also on the sharpness of the angular distribution. For example, the flux is shown in three-dimensional polar coordinates in Figure 3. The total flux of the product is proportional to neither the volume nor the surface area of the lobe shown in the figure. Rather, it is proportional to the signal at a fixed desorption angle. Here, the relation between the mass signal, the total flux of desorbing species, and the sharpness of the angular distribution is discussed.

First, the angular distribution is assumed to be in the following form.

$$f(\theta, \phi) = [\cos(\theta - \theta_o)]^{n\cos\phi\cos\phi + m\sin\phi\sin\phi} \qquad (3)$$

θ is the polar angle, θ_o is the collimation angle, and ϕ is the azimuth angle around the polar axis redefined at $\theta = \theta_o$. n is the power to show the sharpness of the angular distribution at

the fixed azimuth of $\phi = 0°$ and m is the other power at the azimuth perpendicular to the former. The signal intensity observed at the angle (θ, ϕ), $I(\theta, \phi)$, is

$$I(\theta, \phi) = I_0[\cos(\theta - \theta_o)]^{n\cos\phi\cos\phi + m\sin\phi\sin\phi} \quad (4)$$

I_0 is the signal at the collimation angle ($\theta = \theta_o$). The integration of the above quantity yields the total flux of the desorbing molecules, Q.

$$Q = (1/2\pi)I_0\int_0^{2\pi} d\phi \int_0^1 [\cos(\theta - \theta_0)]^{n\cos\phi\cos\phi + m\sin\phi\sin\phi} d(\cos\theta) \quad (5)$$

$$= I_0(n+1)^{-1/2}(m+1)^{-1/2} \quad (6)$$

This result is useful to compare the total flux of desorbing species with different angular distributions. The total flux in eq 6 is proportional to the observed signal I_o at the collimation angle but inversely proportional to the parameter of sharpness $(n+1)^{1/2}(m+1)^{1/2}$. In other words, I_o would be proportional to the parameter of $(n+1)^{1/2}(m+1)^{1/2}$ when the total flux Q is kept constant and the angular distribution is different. This was once described by Comsa and David.[29] The signal in angle-resolved form increases linearly with the increasing total flux of the desorbing species, when the angular distribution remains invariant. This is the case in the present work.

References and Notes

(1) Matsushima, T. *Heterogeneous Chem. Rev*. **1995**, *2*, 51.
(2) Yamanaka, T.; Moise C.; Matsushima, T. *J. Chem. Phys*. **1997**, *107*, 8138.
(3) Cao, G.; Seimiya, Y.; Ohno, Y.; Matsushima, T. *Chem. Phys. Lett.* **1998**, *294*, 419.
(4) Engel, T.; Ertl, G. *Adv. Catal*. **1979**, *28*, 1.
(5) Becker, A.; Cowin, J. P.; Wharton, L.; Auerbach, D. J. *J. Chem. Phys.* **1977**, *67*, 3394.
(6) Allers, K.-H.; Pfnür, H.; Feulner P.; Menzel, D. *J. Chem. Phys.* **1994**, *100*, 3985.
(7) Coulston, G. W.; Haller, G. L. *J. Chem. Phys.* **1991**, *95*, 6932.
(8) Brown, L. S.; Benasek, S. L. *J. Chem. Phys*. **1985**, *82*, 2110.
(9) Matsushima, T.; Yamanaka, T.; Moise, C. *Trends Chem. Phys*. **1996**, *4*, 1.
(10) Ohno, Y.; Matsushima, T.; Uetsuka, H. *J. Chem. Phys.* **1994**, 101, *5319*.
(11) Ohno, Y.; Barrera, A.; Rar, A.; Yamanaka, T.; Sugimura, H.; Matsushima, T. *Surf. Sci*. **1996**, *357/358*, 786.
(12) Rar, A.; Sugimura, H.; Barrera, A.; Ohno, Y.; Matsushima, T. *Surf. Sci*. **1996**, *348*, 77.
(13) Ohno, Y.; Yamanaka, T.; Akiyama, H.; Seimiya, Y.; Matsushima, T. *Appl. Surf. Sci*. **1997**, *121/122*, 567.
(14) Stefanov, P. K.; Ohno, Y.; Yamanaka, T.; Seimiya, Y. Kimura, K.; Matsushima, T. *Surf. Sci.* **1998**, *416*, 305.
(15) Matsushima, T.; Mussett, C. G.; White, J. M. *J. Catal*. **1976**, *41*, 197.
(16) Matsushima, T. *Bull. Chem. Soc. Jpn.* **1978**, *51*, 1956.
(17) Glochet, A.; White, J. M. *J. Catal*. **1978**, *53*, 266.
(18) Ehsasi, M.; Matloch, O.; Frank, O.; Block, J. H.; Christmann, K.; Rys, F. S.; Hirschwald, W. *J. Chem. Phys*. **1989**, *91*, 4949.
(19) Engel, T.; Ertl, G. *J. Chem. Phys*. **1978**, *69*, 1267.
(20) Campell, C. T.; Ertl, G.; Kuipers, H.; Segner, J. *J. Chem. Phys.* **1980**, *73*, 5862.
(21) Reutt-Robey, J. E.; Doren, D. J.; Chabal, Y. J.; Christman, S. B. *Phys. Rev. Lett*. **1988**, *61*, 2778.
(22) Matsushima, T.; Akiyama, H.; Lesar, A.; Sugimura, H.; Gonzalo Torre, E. D.; Yamanaka, T.; Ohno, Y. *Surf. Sci*. **1997**, *386*, 24.
(23) Matsushima, T.; Ohno, Y.; Rar, A. *Surf. Sci*. **1993**, *293*, 145.
(24) Yamanaka, T.; Ohno, Y.; Lesar, A.; Matsushima, T.; Moise, C. *Surf. Sci*. **1996**, *357/358*, 759.
(25) Ohno, Y.; Sanchez, J. R.; Lesar, A.; Yamanaka, T.; Matsushima, T. *Surf. Sci*. **1997**, *382*, 221.
(26) Cao, G.; Seimiya, Y.; Matsushima, T. *J. Mol. Catal*. **1999**, *141*, 63.
(27) Comsa, G.; David, R.; Shumacher, B. J. *Rev. Sci. Instrum*. **1981**, *52*, 789.
(28) Comsa, G.; David, R.; Schumacher, B. J. *Surf. Sci*. **1979**, *85*, 45.
(29) Comsa, G.; David, R. *Surf. Sci. Rep.* **1985**, *5*, 145.
(30) Alavi, A.; Hu, P.; Deutsch, T.; Luigi, P. L.; Hutter, J. *Phys. Rev. Lett*. **1998**, *80*, 3650.
(31) Sowa, E. C.; von Hove, M.A.; Adams, D. L. *Surf. Sci.* **1988**, *199*, 174.
(32) Finnis, M. W.; Heine, V. *J. Phys.* **1974**, *F4*, L37.
(33) Matsushima, T.; Yamanaka, T.; Ohno, Y. *Sci. Rep. RITU* **1997**, *A44*, 215.
(34) Farias, D.; Patting, M.; Rieder, K. H. *Surf. Sci.* **1997**, *385*, 115.
(35) Wang Hong; Tobin, R. G.; Lambert, D. K.; DiMaggio, C. L.; Fisher, G. B. *Surf. Sci.* **1997**, *372*, 267.
(36) Henderson, M. A.; Szabo A.; Yates, J. T., Jr. *J. Chem. Phys.* **1989**, *91*, 7245.
(37) Siddiqui, H. R.; Guo, X.; Cherkendorff, I.; Yates, J. T., Jr. *Surf. Sci.* **1996**, *349*, 119.
(38) Gomer, R. *Rep. Prog. Phys*. **1990**, *53*, 917.
(39) Gland, J. L. *Surf. Sci.* **1980**, *93*, 487.
(40) Gland, J. L.; Sexton, B. A. Fisher, G. B. *Surf. Sci.* **1980**, *95*, 587.
(41) Rar, A.; Matsushima, T. *Surf. Sci*. **1994**, *318*, 89.
(42) Imbihl, R. *Prog. Surf. Sci.* **1993**, *44*, 185.
(43) Ertl, G.; Norton, P. R.; Rüstig, *J. Phys. Rev. Lett.* **1982**, *49*, 171.
(44) Akiyama, H.; Moise, C.; Yamanaka, Y.; Jacobi K. Matsushima, T. *Chem. Phys. Lett.* **1997**, *272*, 219.
(45) Nettesheim, S.; von Oertzen, A.; Rotermund H. H.; Ertl, G. *J. Chem. Phys.* **1993**, *98*, 9977.
(46) von Oertzen, A.; Rotermund, H. H.; Nettesheim, S. *Surf. Sci.* **1994**, *311*, 322.
(47) Seimiya, Y.; Cao, G.; Ohno, Y.; Yamanaka, T.; Matsushima, T.; Jacobi, K. *Surf. Sci. Lett.* **1998**, *415*, 988.
(48) Uetsuka, H.; Watanabe, K.; Kunimori, K. *Chem. Lett.* **1995**, 633.
(49) Watanabe, K.; Uetsuka, H.; Ohnuma, H.; Kunimori, K. *Catal. Lett.* **1997**, *47*, 17.
(50) Watanabe, K.; Ohnuma, H.; Uetsuka, H.; Kunimori, K. *Surf. Sci.* **1996**, *368*, 366.
(51) Uetsuka, H.; Watanabe, K.; Ohnuma, H.; Kunimori, K. *Chem. Lett.* **1996**, 227.
(52) Uetsuka, H.; Watanabe, K.; Kunimori, K. *Surf. Sci*. **1996**, *363*, 73.
(53) Watanabe, K.; Ohnuma, H.; Kimpara, H.; Uetsuka, H.; Kunimori, K. *Surf. Sci.* **1998**, *402−404*, 100.
(54) Mantell, D. A.; Ryali, S. B.; Haller, G. L.; Fenn, J. B. *J. Chem. Phys.* **1983**, *78*, 4250.
(55) Yeo, Y. Y.; Lattuone, L.; King, D. A. *J. Chem. Phys.* **1997**, *106*, 392.